Proceedings of the Canadian Society for Mechanical Engineering International Congress 2021

CSME Congress 2021

June 27-30, 2021, Charlottetown, PE, Canada

Research on Electronic Differential Control Strategy of Distributed Electric Drive Vehicle based on Torque Optimal Distribution

Yangqing Liu[1], Baohua Wang[1]*, Yuping He[2]

School of Automotive Engineering, Hubei University of Automotive Technology, Shiyan, China

[2]Department of Automotive and Mechatronics Engineering, University of Ontario Institute of Technology, Oshawa, Canada

***Abstract*—**To improve the differential performance and lateral stability of distributed drive electric vehicles, this paper proposes an electronic differential control strategy for rear-wheel independent drive electric vehicles based on target torque secondary distribution. Firstly, according to the ideal motion states of the vehicle, the linear quadratic regulator (LQR) is used to calculate the additional required yaw moment, then, the orthogonal experimental method is applied to optimize the LQR parameters, and the target torque is allocated for the first time. Secondly, the target torque is redistributed by designing the functional relationship between the wheel sliding rate and the torque correction coefficient. Finally, the dynamics characteristics of the distributed electric vehicle with electronic differential control is simulated and analyzed in comparison with the traditional mechanical differential. The results show that the proposed electronic differential control strategy can not only achieve differential control well, but also the side slip angle and the yaw angle are reduced by up to 36.3% and 88.8% respectively, compared with the traditional vehicle. The proposed electronic differential control strategy ensures that the wheel sliding rate is always in the optimal sliding rate range, and greatly improves the vehicle lateral stability.

Keywords-distributed electric vehicle; electronic differential; sliding rate; control strategy

I. Introduction

Distributed electric vehicles allocate a drive motor to each drive wheel. Compared with traditional centralized drive vehicles, it has the advantages of compact structure, high power transmission efficiency, and rapid response [1]. However, due to the cancellation of the mechanical differential, when the vehicle operates on a curved path, the uncoordinated drive wheel torques can easily lead to serious wheel wear, and even side slip in severe cases. Therefore, for distributed drive electric vehicles, it is particularly important to design an efficient and practical electronic differential control strategy.

Several scholars have conducted research on electronic differential control methods. Folgado et al. imitated the principle of traditional mechanical differential and proposed an electronic differential control strategy based on the equal distribution of torque. Although the differential function could be achieved, the sliding rate of the driving wheels was not monitored, and the running performance of the vehicle under complex road conditions could not be guaranteed [2-4]. Al-Fiky et al. regarded reducing wheel sliding rate and avoiding motor torque oversaturation as constraints, proposing an adaptive electronic differential strategy based on equal torque distribution. Although the wheel sliding rate was

Fund Program: Natural Science Foundation of China (52072116) ; Key R&D Project of Hubei Province (2020BAB141) ;

About the author: Yangqing Liu (1996-), female, graduate student, engaged in research on stability control of electric vehicles. E-mail: 157599990@qq.com

*Corresponding author: Baohua Wang, male, Professor, Ph.D., Research direction: Vehicle Dynamics and Control. E-mail:wbhbenz@126.com

reduced, a more reasonable driving torque distribution method was not adopted, thus the vehicle lateral stability is poor [5,6]. Daya et al. used the Ackermann geometry to determine the target speed of each wheel, using closed-loop control to realize the torque distribution of the driving wheels, then, adjusted the speed to achieve the differential effect. However, this strategy was only suitable for low-speed conditions with no wheel side slip. When the side slip angle was large, the control effect was not effective [7,8]. Hua et al. combined the electronic differential and yaw stability control, using the deviation between the yaw rate, side slip angle of the center of mass and the ideal value to design an additional yaw moment controller. At the same time as the differential functioned, the lateral stability had also been improved. However, the research only focused on roads with high adhesion coefficients, and did not consider vehicle operating conditions on roads with low adhesion coefficients [9-11]. He et al. used hierarchical strategy to combine the torque control of the vehicle with the sliding rate control, and adjusted the additional yaw moment by real-time estimation of the sliding rate of the driving wheel, then, adjusted the output torque of the drive motor to ensure that the sliding rate could be controlled within the optimal range when turning. This method had improved the performance of vehicle's differential and lateral stability, but the design was complicated, and parameters of control strategy had not been further optimized, so the result couldn't reach the best effect [12-14].

To address the aforementioned questions, a distributed two-rear-wheel independent drive electric vehicle is taken as the research object, and the following three models are generated:

(a) a linear 2-DOF vehicle model;

(b) a permanent magnet synchronous motor (PMSM) model;

(c) a nonlinear model developed using Trucksim.

The PMSM model is generated using Matlab /Simulink to serve as the power source of the distributed electric drive vehicle; with TruckSim software, a virtual distributed vehicle model is constructed, which consists of suspension system, brake system, tire model, etc. Through the interaction between Simulink and TruckSim, the co-simulation model of distributed drive electric vehicle is fabricated. In addition, the linear 2-DOF vehicle model and LQR controller are also generated and designed using MATLAB/Simulink, which are used for the design of the electronic differential control strategy. Based on the deviation between the actual and the ideal value of the vehicle side slip angle and yaw rate obtained by the linear vehicle model, the additional yaw moment is calculated and the torque difference between the two rear wheels is determined to realize the rear wheels' rotating speed difference. At the same time, the orthogonal test method is used to optimize the LQR parameters to improve the lateral stability of the vehicle.

II. Permanent Magnet Synchronous Motor based Drive System Model

A. Permanent Magnet Synchronous Motor Model

In the PMSM modelling, it is assumed that the saturation of the motor core is negligible; the eddy current phenomenon and hysteresis loss phenomenon in the motor don't affect the performance of the motor; the three-phase currents of the stator are symmetrical with each other, and have a standard sine wave shape. After coordinate system transformation, the mathematical model under the synchronous rotating coordinate system of PMSM is generated.

The stator voltage is determined by,

$$\begin{cases} u_d = R_s i_d + L_d \dfrac{di_d}{dt} - \omega_e L_q i_q \\ u_q = R_s i_q + L_q \dfrac{di_q}{dt} + \omega_e (L_d i_d + \psi_f) \end{cases} \tag{1}$$

The stator flux is given by,

$$\begin{cases} \psi_d = L_d i_d + \psi_f \\ \psi_q = L_q i_q \end{cases} \tag{2}$$

The electromagnetic torque is calculated as,

$$T_e = 1.5 p_n \left[\psi_f i_q + (L_d - L_q) i_d i_q \right] \tag{3}$$

The dynamic equation of the motor is cast as,

$$J \frac{d\omega_m}{dt} = T_e - T_L - B\omega_m \tag{4}$$

The notation of formulas (1)-(4) are provided in Appendix 1

B. Vector Control Strategy of Permanent Magnet Synchronous Motor

The basic idea of vector control is to simulate the law of DC motor torque control on a three-phase AC motor, that is, under the rotor field orientation coordinates, through coordinate transformation, the stator current vector i_s of a three-phase AC motor is decomposed into the excitation current component i_q, which produces the flux and the torque current component i_d, which in turn produces the torque. The two current components are perpendicular to each other and they are independent. By this way, the torque control of the AC motor is transformed into the control of the amplitude and spatial position of the stator current vector, and the three-phase AC permanent magnet synchronous motor can be controlled as easily as the DC motor.

If the value of i_d is set to 0, then equation (3) could be simplified as,

$$T_e = 1.5 P_n \psi_f i_q \quad (5)$$

where T_e is proportional to the magnitude of i_q. As long as appropriate i_q is adjusted, the target T_e could be obtained. The control strategy is simple, clear and easy to be implemented. Therefore, the vector control strategy of $i_d = 0$ is chosen as the control scheme of PMSM drive system in this paper. The control schematic diagram is shown in Fig.1.

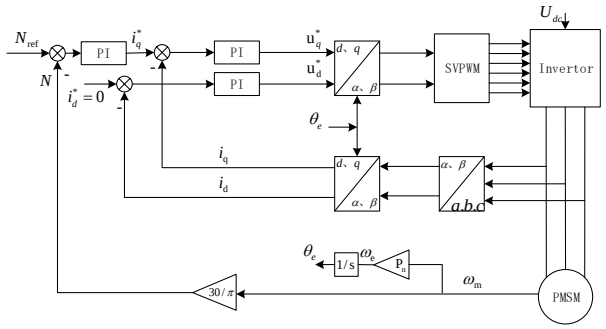

Fig.1: $i_d = 0$ vector control principle block diagram.

As can be seen from Fig.1, the system is composed of a double closed-loop control system with an inner current loop and an outer speed loop. It mainly includes: coordinate transformation module, speed current regulator module, SVPWM (stator voltage pulse width modulation?) module and speed position acquisition module.

C. PMSM Response Performance Analysis based on $i_d = 0$ Vector Control Strategy

Based on the Simulink platform, the $i_d = 0$ control mode is simulated and analyzed. The rated voltage of PMSM is 220V, the phase resistance R is 0.025Ω, the inductances L_d and L_q of the vertical axis are 0.2mH and 0.47mH respectively, the permanent magnet flux linkage ψ_f is 0.1827, the moment of inertia J is 0.02kg · m^2, and the number of pole pairs is 4.

The motor starts at a speed of 500r/min with no load, the speed rises to 1000r/min at 0.2s, and the load is suddenly added 30Nm at 0.6s. The simulation time is 1s. And the simulation results obtained are shown in Fig.2.

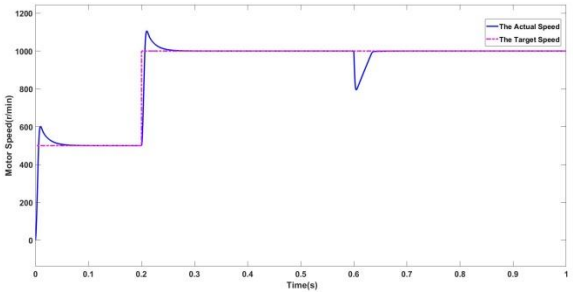

(a) Motor Speed

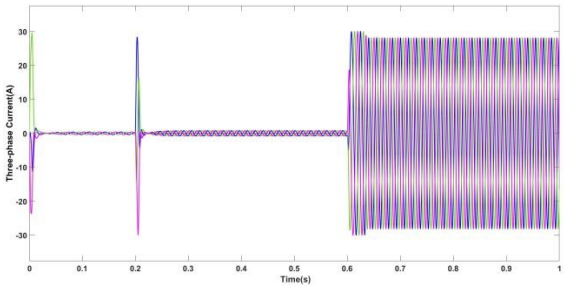

(b) Three-phase Current

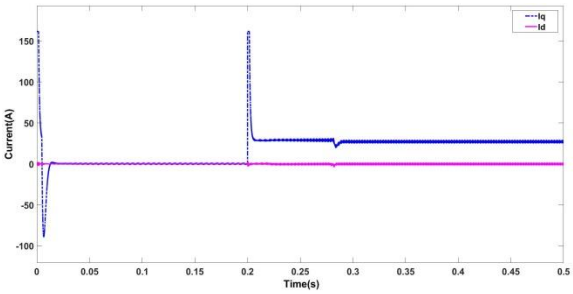

(c) Direct Axis and Quadrature Axis Current of Motor

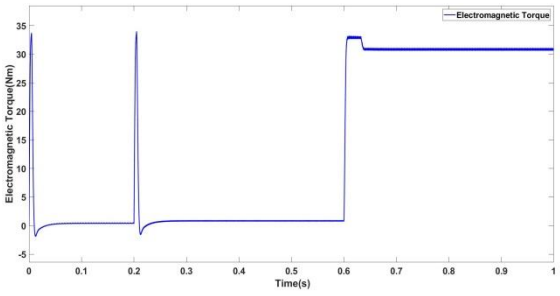

(d) Electromagnetic Torque

Fig.2: PMSM Response Performance Analysis based on $i_d = 0$ Vector Control Strategy.

As can be seen from Fig.2(a), the motor is set at 500 r/min before 0.2s, and the speed of about 0.01s follows the set value and maintains stable operation. At 0.2s, the

target speed suddenly increases to 1000 r/min, and the actual speed also quickly reaches the new stable value. When the load of 30 Nm is suddenly added at 0.6s, the motor speed drops from 1000 r/min to 800 r/min. However, by adjusting the speed, the actual speed quickly recovered and remained stable within 0.04s.

As can be seen from Fig. 2(b), when the motor is started, the starting current is large. This is because in the initial stage, the rotating magnetic field has not yet formed and the induced electromotive force has not been generated in the stator windings. At this time, the external voltage will all act on the smaller stator windings, resulting in a larger current. When the motor begins to enter the stable operation stage, the induction electromotive force begins to form in the stator winding, and the stator current rapidly decreases, and gradually presents a sinusoidal trend. At the time of 0.2s, the target speed increases, however, the rotor speed has not reached the given value, so the current increases largely. The current decreases rapidly after the stable operation of the motor. At the moment of 0.6s, when the load is suddenly added, the motor speed will suddenly drop. In order to keep the speed constant, the current will increase to maintain a new stable state. Overall, the current has a fast response speed and good stability

As can be seen from Fig.2(c), the direct axis current i_d is basically 0 due to the control mode of $i_d = 0$. From Fig.2(d), the response speed of the electromagnetic torque is fast, and the change of the electromagnetic torque is proportional to the change of the quadrant axis current, which is in line with the theoretical analysis.

According to the above simulation results, it could be seen that without payload, the motor start speed response is faster, the overshoot is small, and the operation is stable. After adding load disturbance, the electromagnetic torque response is fast, and the dynamic performance and anti-interference ability of the system are strong. Therefore, it could be used as the wheel drive motor of electric vehicle.

III. Distributed Electric Vehicle Model

A. 2-DOF Model

In order to obtain the ideal side slip angle and yaw rate of the vehicle at any time during the process of driving, the ideal reference vehicle model should be generated firstly. In this paper, the linear 2-DOF vehicle model is taken as the reference model of two rear-wheel distributed drive electric vehicle.

The 2-DOF model is shown in Fig.3. Let the origin of the vehicle coordinate system be coincident with the center of mass of the vehicle; *x* axis points to the front parallel to the ground, *y* axis points to the left of the driver, and *z* axis points to the top through the center of mass [15]. According to Newton's second law, the governing equations of motion of the 2-DOF linear vehicle model are generated as follows.

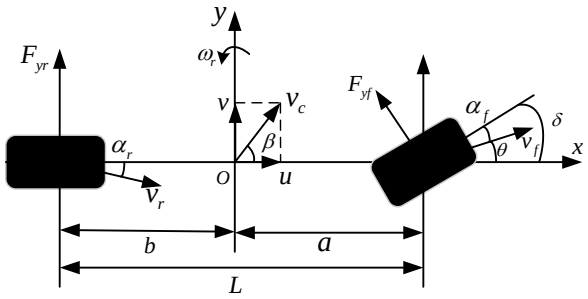

Fig.3: Vehicle linear two-degree-of-freedom dynamics model.

$$\begin{cases} \Sigma F_y = F_{yf}\cos\delta + F_{yr} \\ \Sigma M_z = aF_{yf}\cos\delta - bF_{yr} \end{cases} \tag{6}$$

$$\begin{cases} \Sigma F_y = k_1\left(\beta + \frac{a\omega_r}{u} - \delta\right) + k_2\left(\beta - \frac{b\omega_r}{u}\right) \\ \Sigma M_z = ak_1\left(\beta + \frac{a\omega_r}{u} - \delta\right) - bk_2\left(\beta - \frac{b\omega_r}{u}\right) \end{cases} \tag{7}$$

$$\begin{cases} (k_1 + k_2)\beta + \frac{1}{u}(ak_1 - bk_2)\omega_r - k_1\delta = m(\dot{v} + u\omega_r) \\ (ak_1 - bk_2)\beta + \frac{1}{u}(a^2k_1 + b^2k_2)\omega_r - ak_1\delta = I_z\dot{\omega}_r \end{cases} \tag{8}$$

where, the state-space equation is

$$\begin{bmatrix} \dot{\beta} \\ \dot{\omega}_r \end{bmatrix} = \begin{bmatrix} \frac{k_1 + k_2}{mu} & \frac{ak_1 - bk_2}{mu^2} - 1 \\ \frac{ak_1 - bk_2}{I_z} & \frac{a^2k_1 + b^2k_2}{I_z u} \end{bmatrix} \begin{bmatrix} \beta \\ \omega_r \end{bmatrix} + \begin{bmatrix} -\frac{k_1}{mu} \\ -\frac{ak_1}{I_z} \end{bmatrix} \delta \tag{9}$$

The notation of Fig.3 are provided in Appendix 1

B. TruckSim Model

TruckSim is a commercial software package specifically designed for dynamic simulation of large commercial vehicles, namely VehicleSim (VS) Lisp. It integrates three functions of vehicle modeling, condition simulation and data analysis, and is composed of condition parameter setting, model solving and result post-processing. Different from traditional modeling software based on structural design, vehicle modeling by TruckSim only needs to be defined according to the

performance and characteristic parameters of each system to build a vehicle model with a high degree of fidelity to the actual vehicle.

For the distributed two-rear-wheel independent drive electric vehicle, the configuration of the vehicle can be defined as S_S，where S indicates a solid axle and the underline (_) represents a separation of axle groups. Thus, as the configuration indicated, the distributed two-rear-wheel independent drive electric vehicle consists of two solid axles. VS Lisp takes an input as the description of the distributed two-rear-wheel independent drive electric vehicle configuration, such as force vectors and the body DOF. With that, VS Lisp derives equations of motion in terms of the ordinary differential equations and generates a computer source code (C or Fortran) to solve them.

In this research, the numerical simulations based on the 2-DOF model and the PMSM model are performed using MATLAB software. The virtual distributed two-rear-wheel independent drive electric vehicle was built based on Trucksim software. The PMSM drive model is combined with the virtual distributed drive electric vehicle for co-simulation. The co-simulation model is shown in Fig.4.

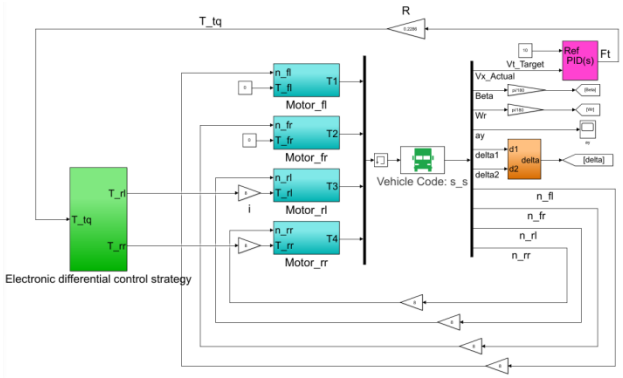

Fig.4: Co-simulation model of distributed electrically drive vehicle.

C. Vehicle Model Validation

To ensure that the distributed drive electric vehicle model is basically consistent with the traditional vehicle model in Trucksim software, the result comparisons between the electric vehicle and the traditional vehicle are carried out respectively. Validating conditions are as follows: the vehicle speed is 40km/h, the road adhesion coefficient is 0.85, the step turn maneuvers and fishhook maneuvers are conducted respectively.

a. Step turn maneuver

The steering maneuver starts from the first second and the peak angle is 180deg, the angular ratio of the steering system is 1:25.The responses of yaw rate, side slip angle and trajectory of the center of mass are shown in Figure 5 (a)-(d).

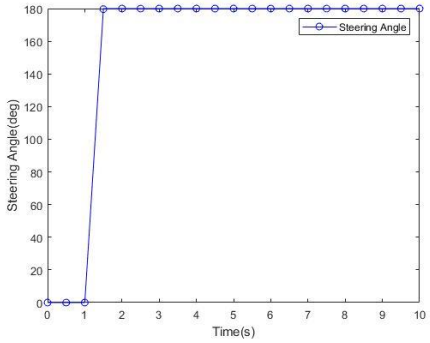

(a)Steering wheel Angle

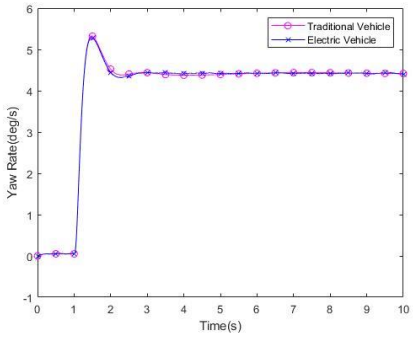

(b) Yaw Rate

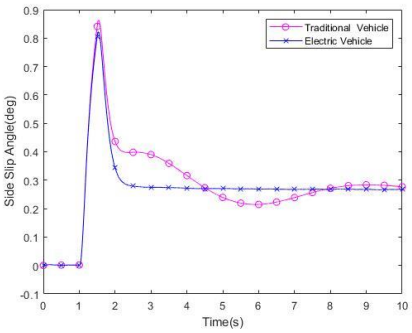

(c) Side Slip Angle

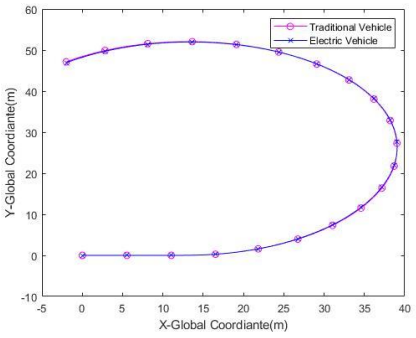

(d) Trajectory

Fig.5: Response comparisons of vehicle under step turn maneuver

As can be seen from Fig. 5, under the step turn maneuvers of 40km/h, the yaw rate of distributed drive electric vehicle has a high degree of fidelity, and almost completely coincides with the traditional vehicle after 7th second. In the process of steering wheel alignment, the side slip angle of centroid of a traditional vehicle fluctuates greatly, while the response of the distributed electric vehicle is more smooth due to the cancellation of a series of transmission components. The trajectories of the two vehicles' center of mass also almost completely overlap. The coincidence degree of side slip angle, yaw rate and centroid trajectory are all above 90%.

b. Fishhook maneuver

The input peak angle of steering wheel is 200deg. The responses in terms of yaw rate, side slip angle and trajectory of the center of mass are shown in Figure 6 (a)-(d).

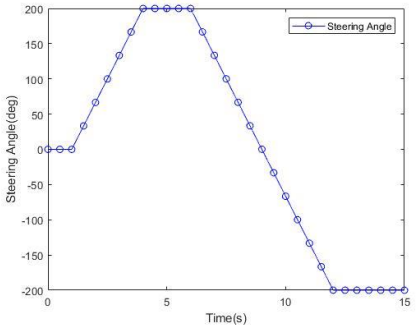

(a) Steering Angle

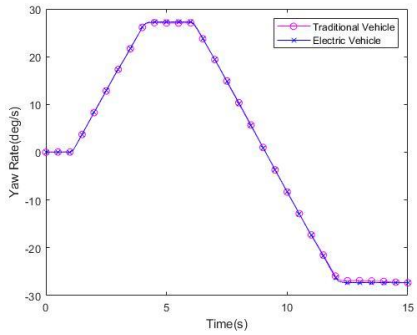

(b)Yaw Rate

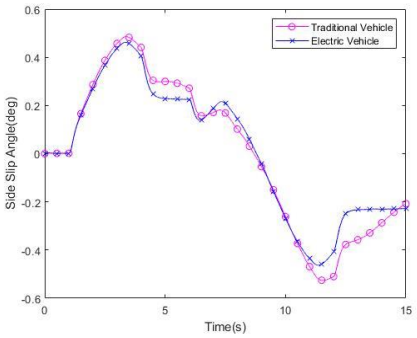

(c)Side Slip Angle

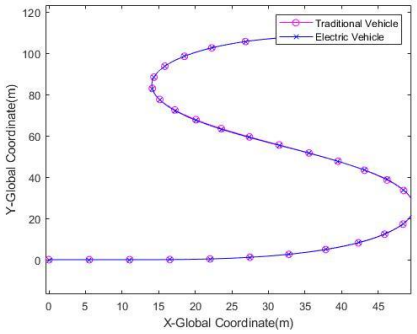

(d) Trajectory

Fig.6: Response comparisons of vehicle under fishhook maneuver.

The vehicle speed is 40km/h and the road surface friction coefficient, μ, is 0.85. As can be seen from Fig. 6, the yaw rate and the centroid travel trajectory of distributed drive electric vehicle almost completely coincide with those of the traditional vehicle, and the side slip angle of centroid of electric vehicles fluctuates less than that of traditional vehicles. The coincidence degree of the three performance parameters is all above 95%.

In summary, the similarity between the distributed drive electric vehicle model and the traditional vehicle model in Trucksim is more than 90%, which has a high reliability and can meet the requirement for developing the electronic differential control strategy.

III. DESIGH Of ELECTRONIC DIFFERENTIAL CONTROLLER

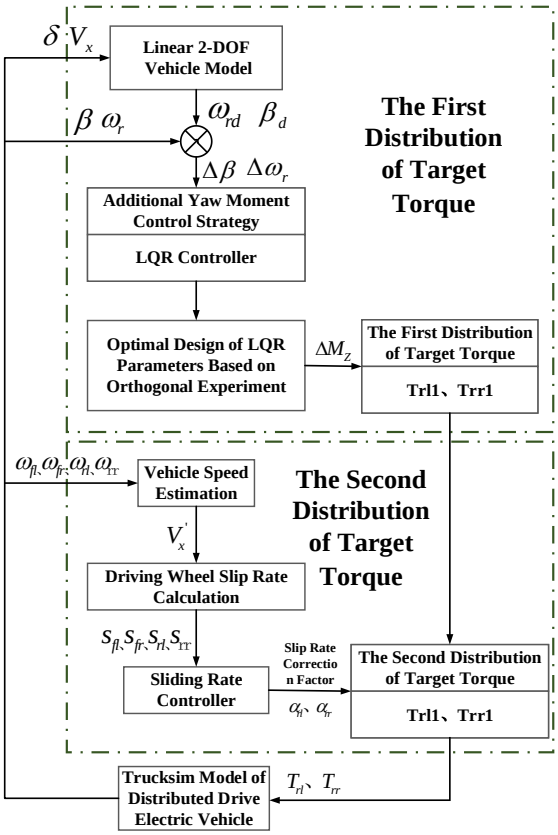

Fig.7: Proposed design framework of control strategy for electronic differential of distributed drive electric vehicle.

The traditional mechanical differential coordinates the rotations of the planetary gears inside the differential based on the tangential forces between the wheels and the road surface to achieve the differential effect. Similarly, for the electronic differential, although the final expression of the differential falls on the different speeds of the inner and outer wheels, if we want to directly control the speed to achieve the differential, the target speed of each wheel would be controlled by closed loop speed. Although the differential effect could be realized theoretically, the speed of each wheel is strictly constrained by the steering geometry, and they are independent of each other. The control of the driving torque of each driving wheel is also independent of each other, and it is impossible to guarantee the coordinated distribution of the driving torque of the whole vehicle. Therefore, in order to achieve a stable and reliable differential effect, differential control essentially needs to be carried out by perceiving the interaction force between the wheels and the ground and by coordinating the distribution of the driving torque of the inner and outer driving wheels.

The proposed design framework of the electronic differential control strategy is shown in Fig 7, which uses a hierarchical control method using two levels of target torque distribution. In upper level, an additional yaw moment controller is designed using the LQR technique, which calculates the additional yaw moment. Then, an orthogonal experimental method is used to optimize the design of LQR parameters and distributes the target torque of the driving wheels for the first time, making the actual state of the vehicle closer to the ideal state. The torque distribution should not only meet the vehicle's dynamic demand and differential control, but also take full account of the restriction of road surface adhesion conditions. When the driving torque applied to the wheels is greater than the limit of road adhesion, the wheels will slip greatly, which degrades tractive performance and lateral stability of the vehicle under the conditions of low adhesion coefficient road and high-speed driving. Therefore, the sliding rate of both driving wheels is introduced to allocate the second target torque of the driving motor. In the lower level, the sliding rate controller is fabricated, which aims to keep the sliding rate of the driving wheels in the best sliding rate range. It monitors the sliding rate of each wheel in real time, establishes the functional relationship between the torque correction coefficient and the sliding rate, and adjusts the target torque of the driving wheels to realize the second distribution of torque. The notation of Fig.7 are provided in Appendix 1

A. Design of Yaw Moment Control Strategy Using LQR

When the longitudinal velocity u of the vehicle remains constant, the vehicle will reach a steady state when $\dot{v} = 0\ and\ \dot{\omega}_r = 0$. With the 2-DOF linear vehicle model, the ideal yaw rate and side slip angle can be obtained as:

$$\omega_{rd} = \frac{u\delta}{L(1+Ku^2)} \tag{10}$$

$$\beta_d = 0 \tag{11}$$

where L is the wheelbase, K is the understeer coefficient and $K = \frac{m}{L^2}(\frac{a}{k_2} - \frac{b}{k_1})$. The calculation formula for the lateral acceleration at the center of mass of the vehicle is:

$$a_y = \dot{v} + u\omega_r \tag{12}$$

Considering the limitations of road adhesion conditions, the lateral acceleration can't exceed the maximum lateral

acceleration kμg [16] provided by the ground:

$$a_y \le k\mu g, k = 0.85 \tag{13}$$

Thus, the upper limit of the vehicle yaw rate can be determined as:

$$\omega_{rmax} = 0.85\frac{\mu g}{u} \tag{14}$$

Therefore, the ideal states of the 2-DOF linear vehicle model can be expressed as:

$$\begin{cases} \omega_{rd} = min\left\{\left|\frac{0.85\mu g}{u}\right|, |\omega_r|\right\} sgn(\omega_r) \\ \beta_d = 0 \end{cases} \tag{15}$$

According to equation (9), the state space equation of the 2-DOF linear vehicle model is given by:

$$\begin{bmatrix} \dot{\beta} \\ \dot{\omega}_r \end{bmatrix} = A\begin{bmatrix} \beta \\ \omega_r \end{bmatrix} + B\delta \tag{16}$$

where $A = \begin{bmatrix} \frac{k_1+k_2}{mu} & \frac{ak_1-bk_2}{mu^2} - 1 \\ \frac{ak_1-bk_2}{I_z} & \frac{a^2k_1+b^2k_2}{I_z u} \end{bmatrix}$, $B = \begin{bmatrix} -\frac{k_1}{mu} \\ -\frac{ak_1}{I_z} \end{bmatrix}$.

When the additional yaw moment ΔM_Z is applied, the formula (16) becomes:

$$\begin{bmatrix} \dot{\beta} \\ \dot{\omega}_r \end{bmatrix} = A\begin{bmatrix} \beta \\ \omega_r \end{bmatrix} + B\delta + B_1\Delta M_Z \tag{17}$$

where $B_1 = \begin{bmatrix} 0 \\ \frac{1}{I_Z} \end{bmatrix}$.

Subtracting formula (16) and formula (17), the state space equations in terms of $\Delta\dot{\beta}$、$\Delta\dot{\omega}_r$ can be obtained as follows:

$$\begin{bmatrix} \Delta\dot{\beta} \\ \Delta\dot{\omega}_r \end{bmatrix} = \begin{bmatrix} \frac{k_1+k_2}{mu} & \frac{ak_1-bk_2}{mu^2} - 1 \\ \frac{ak_1-bk_2}{I_z} & \frac{a^2k_1+b^2k_2}{I_z u} \end{bmatrix} \begin{bmatrix} \Delta\beta \\ \Delta\omega_r \end{bmatrix} + \begin{bmatrix} 0 \\ \frac{1}{I_z} \end{bmatrix} \Delta M_Z \tag{18}$$

Assume $x = \begin{bmatrix} \Delta\beta \\ \Delta\omega_r \end{bmatrix}$, $u = [\Delta M_Z]$, then the equation (18) can be expressed as a general form.

$$\dot{x} = Ax + B_1 u \tag{19}$$

The verification shows that the time invariant linear system $\dot{x} = Ax + B_1 u$ is fully controllable, and its performance index within the infinite time range is defined as,

$$J = \frac{1}{2}\int_0^\infty [x^T(t)Qx(t) + u^T(t)Ru(t)]dt \tag{20}$$

where R is the input vector weight matrix, and Q is the state vector weight matrix. Assume $Q = \begin{bmatrix} q_{11} & 0 \\ 0 & q_{22} \end{bmatrix}$, $R = [r_{11}]$, the element q_{11} represents the weight coefficient of the vehicle side slip angle, q_{22} represents the weight coefficient of the yaw rate, and r_{11} represents the weight coefficient of the additional yaw moment. According to different vehicle velocities and driving conditions, the consideration of the focus of each weight coefficient is different. It is generally believed that when the vehicle is running at low speeds, in order to meet the requirements of maneuverability, it should be as far as possible to maintain zero-mass center side slip angle, q_{11} should be much larger than q_{22}; while driving at medium and high speeds, the emphasis should focus on improving the lateral stability of the vehicle to reduce for yaw movement, q_{22} should be greater than q_{11}. The optimal control quantity can be expressed as:

$$\Delta M_Z^* = -K_1 x(t) \tag{21}$$

where, $K_1 = R^{-1}B^T P$ is the optimal control feedback coefficient matrix, P is the solution of Riccati equation $PA + A^T P - PBR^{-1}B^T P + Q = 0$, by calling the function lqr() provided in Matlab to solve the above Riccati equation, the additional yaw moment can be obtained, and the first target torque distribution is completed.

B. Optimization of LQR Parameters based on Orthogonal Experiment Design

Although the LQR weight coefficients designed above can realize differential control, the resulting evaluation parameters of vehicle lateral stability are not optimal. Conventionally, the weighting matrices of LQR controllers are determined using trial and error method, which is a time consuming and tedious process. To address this issue, an optimization method using genetic algorithms (GA) was proposed to find desired weighting matrices for LQR controllers [17-19]. However, the GA-based optimization process is not computationally efficient. In this paper, an alternative, i.e., an orthogonal experimental design method, is proposed for determining the LQR weighting matrices. The LQR controller is a linear controller, and the optimal weighting matrices are

vehicle forward speed dependent. Thus, different weighting matrices need to be considered at different vehicle speeds, in order to find a group of relatively optimal weight coefficients, which can not only realize the differential function, but also improve the lateral stability of the vehicle.

Orthogonal experiment is an experiment optimization technology that studies multiple factors and levels. By arranging the experimental factors at the appropriate level and using a standardized orthogonal table for experimental analysis, the best solution can be found through a few experiments [20].

Under the simulated obstacle avoidance testing maneuver recommended by ISO3888-2:2002, the influence of the three factors, i.e., q_{11}, q_{22} and r_{11}, on the stability of the vehicle at a speed of 40km/h is investigated. In the orthogonal experiment, we take two levels of each factor. Since the vehicle is running at a low speed at this time, the deviation between the actual value and the ideal value of the vehicle side slip angle is selected as the evaluation index. The factor levels are shown in Table 1. The orthogonal table $L_4(2^3)$ is selected for the experiment, and the form of the table is shown in Table 2. The experimental scheme and result analysis are shown in Table 3.

TABLE I: Factor Level Table

Level	Factor		
	$A-q_{11}$	$B-q_{22}$	$C-r_{11}$
1	$A_1(85000)$	$B_1(0)$	$C_1(1*10^{-6})$
2	$A_2(90000)$	$B_1(0)$	$C_2(1*10^{-7})$

TABLE II: $L_4(2^3)$ Orthogonal Table

Test No.	1	2	3
1	1	1	1
2	1	2	2
3	2	1	2
4	2	2	1

TABLE Ⅲ: Experimental Scheme and Result Analysis Table

	Factor			evaluation index
	q_{11} (A)	q_{22} (B)	r_{11} (C)	error_Beta(°)
1	$A_1(85000)$	$B_1(0)$	$C_1(1*10^{-6})$	0.246
2	$A_1(85000)$	$B_2(50)$	$C_2(1*10^{-7})$	0.157
3	$A_2(90000)$	$B_1(0)$	$C_2(1*10^{-7})$	0.126
4	$A_2(90000)$	$B_2(50)$	$C_1(1*10^{-6})$	0.251
T_1	0.403	0.372	0.497	
T_2	0.377	0.408	0.283	
$\overline{T_1}$	0.2015	0.186	0.2485	$T = 0.78$
$\overline{T_2}$	0.1885	0.204	0.1415	
R	0.013	0.018	0.107	
S	0.000169	0.000324	0.011449	$S_T = 0.011942$ $S_E = 0.000169$

Note that T represents the sum of data of all experiments; T_i represents the sum of experimental data at the i-th level of each factor; $\overline{T_i}$ represents the average; R is the poor of $\overline{T_i}$; S is the sum of squares, where S_T is the sum of squares of total deviation and S_E is the sum of squares of errors.

The data processing of orthogonal experiment can be divided into two kinds: range analysis and variance analysis. In this research, the variance analysis is adopted. Based on the above experimental results, an analysis of variance table can be listed, as shown in Table 4.

TABLE Ⅳ: Analysis of Variance Table

Source	Quadratic Sum**S**	Degree of Freedom**f**	Mean Sum of Square**V**	**F**Ratio
FactorA	0.000169	1	0.000169	1
FactorB	0.000324	1	0.000324	1.92
FactorC	0.011449	1	0.011449	67.75
FactorE	0.000169	1	0.000169	

Note that the mean sum of square is equal to the square sum divided by the corresponding degree of freedom, and the F ratio is equal to the factor mean square sum divided by the error mean square sum.

According to the principle of variance analysis of orthogonal experiment, the larger the value of F ratio, the higher the degree of influence of the corresponding factor on the experiment [20]. Thus, the priority of the factors can

be arranged according to the size of F ratio. The primary and secondary order of factors are C, B, and A.

The selection of the optimal factor level collocation is based on the order of factors, we choose the optimal level for each factor. As can be seen from Table 5, for factor C, $C_2(1*10^{-7})$ is the best; for factor B, $B_1(0)$ is the best; for factor A, $A_2(9000)$ is the best. That is, the optimal level collocation could be concluded as follows: $C_2(1*10^{-7})$, $B_1(0)$, $A_2(9000)$. Therefore, the relative optimal parameters of LQR under this operating condition should be set as: $r_{11}=1*10^{-7}$、$q_{11}=90000$、$q_{22}=0$. Similarly, the relative optimal parameter values of the vehicle under other operating conditions can be analyzed.

C. Design of Sliding Rate Control Strategy

Based on the driving wheel torque distributed by the LQR yaw moment controller, in addition to meet the power transmission requirements of the vehicle, it is also necessary to fully consider the constraints of the road adhesion conditions. When the driving torque applied to the wheels is greater than the road adhesion limit, the wheels will slip significantly. Therefore, the sliding rate of the driving wheels on both sides is introduced for the lower level target torque distribution of the driving motor, which not only plays the role of electronic differential, but also further improves the lateral stability of the vehicle.

The lower level distribution of the target torque is manipulated by the sliding rate fed back by wheels. The torque correction coefficient α is introduced, and the relationship between α and wheel sliding rate s is shown in Figure 4.

$$\alpha=\begin{cases}0, & 0\le s<15\\ \dfrac{1}{30}s-0.5, & 15<s\le 30\\ 0.5, & 30<s\le 1\end{cases} \tag{22}$$

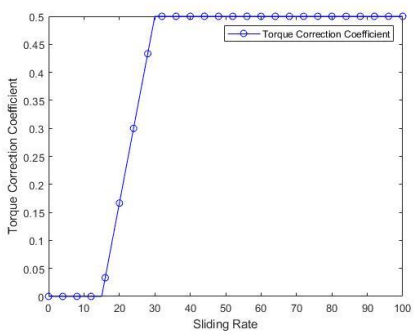

Fig.8: Torque correction coefficient α curve.

When the wheel sliding rate is within a reasonable slip range, that is, less than 15%, the torque correction coefficient α is 0, and the driving torque on both sides is not corrected. When the sliding rate is in the range of [15%, 30%], the correction coefficient α is adjusted to the driving torque according to the rule of formula (19), and the target torque is appropriately reduced. When the slip ratio is greater than 30%, the correction coefficient α is 0.5, which reduces the target torque to half of the original value. At this time, the power of the vehicle should be appropriately sacrificed, and the driving safety should be the primary consideration. Through the lower level torque distribution, no matter what operating conditions the vehicle is in, the torque can be corrected and the lateral stability of the vehicle could be improved.

D. Target Torque Distribution Strategy for Rear Wheel Drive Motors

After calculating the additional yaw moment required by the vehicle through the upper level controller, and monitoring the sliding rate of each drive wheel in real time, the target torque of each drive motor needs to be allocated in the lower level controller.

The upper level distribution of the target torque is implemented as follows: the total demand torque T_t is obtained through the driving motor model, and combined with the additional yaw moment ΔM_Z, the target torque of the driving motor on both sides can be calculated.

$$\begin{cases}T_{r31}=\dfrac{1}{2}(T_t-\Delta M_Z)\\ T_{r41}=\dfrac{1}{2}(T_t+\Delta M_Z)\end{cases} \tag{23}$$

When the wheel sliding rate exceeds a reasonable range, the target torque needs to be adjusted to carry out the lower level torque distribution.

$$\begin{cases}T_{r32}=T_{r31}(1-\alpha_3)\\ T_{r42}=T_{r41}(1-\alpha_4)\end{cases} \tag{24}$$

To date, high fidelity co-simulations have been applied to the design and development of active safety systems of road vehicles [21-22]. To validate the electronic differential controller, a closed-loop differential control is implemented and simulated using the TruckSim and MATLAB/Simulink co-simulation as illustrated in Fig.9.

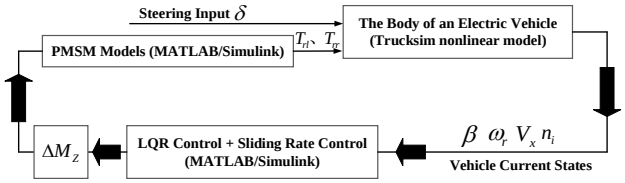

Fig.9: Co-simulation environment with MATLAB-TruckSim for differential controller.

IV. RESULTS AND DISCUSSION

To investigate the differential effect of the electronic differential and the improvement of the lateral stability of the vehicle, the vehicles based on the traditional mechanical differential and the electronic differential are simulated under the maneuvers of double lane change and step turn on high and low road adhesion coefficient, and the simulation results of the two strategies are compared.

A. Simulations under DLC maneuver at low speed

To verify the maneuverability and lateral stability of distributed electric vehicles at low speeds based on the electronic differential control strategy, simulations are carried out in the standard operating conditions of double lane change (DLC) maneuvers of ISO3888-2:2002. The DLC maneuvers are set as follows: the simulated vehicle velocity is 40km/h, and the road adhesion coefficient is 0.85. The results are shown in Figure 10.

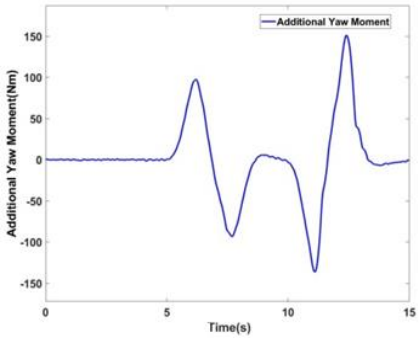

(a) Additional Yaw Moment

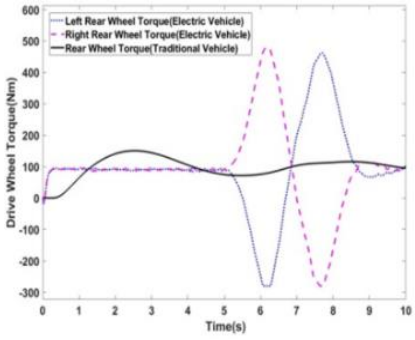

(b) Drive Wheel Torque

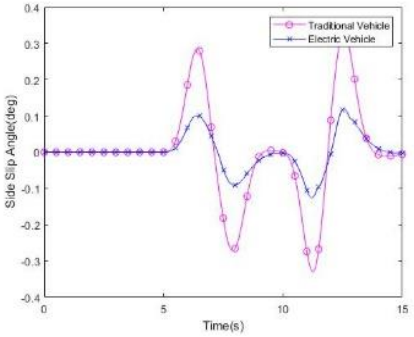

(c) Side Slip Angle

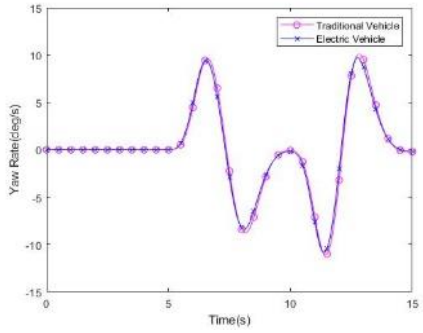

(d) Yaw Rate

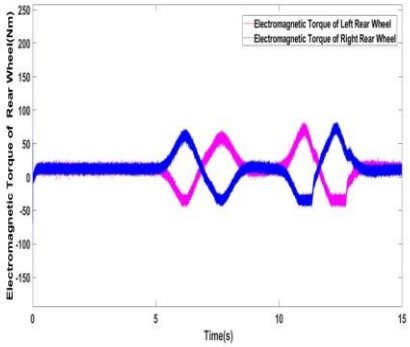

(e) Electromagnetic Torque of Rear Wheel

Fig.10: Characteristic Comparisons of electronic differential control strategy under double lane change maneuver at low speed

TABLE Ⅵ: Comparisons of Simulation Results of Different Strategies under DLC Maneuver at 40km/h

Simulation Parameters	Mechanical differential	Electronic differential	
	Data	Data	Rate of change
β_{max}(deg)	0.33	0.12	-63.7%
ω_{rmax}(deg/s)	10.10	9.70	-4.0%

Due to the torque distribution method based on additional yaw moment, when the vehicle is steering, the

torque difference between the left and right rear driving wheels of the distributed electric vehicle will be generated, and the torque difference will change with the change of vehicle rotation to meet the maneuverability requirements. However, because of the use of mechanical differential, the driving torques of the left and right sides of traditional vehicles are always consistent. The torque response is shown in Fig. 10(b), and the additional yaw moment response is shown in Fig. 10(a). It can be seen from table VI that under the 40km/h DLC maneuver, the vehicle side slip angle and yaw rate based on the traditional mechanical differential are relatively large, and the lateral stability is poor. Since the vehicle can adjust the driving torque on both sides in real time, it can make full use of the attachment conditions of the road to improve vehicle stability under the premise of realizing the differential function. Compared with the mechanical differential, the rate of change of the vehicle side slip angle reaches -63.7 %, improved from 0.33deg to 0.12deg. The yaw rate has also been reduced from 10.1deg/s to 9.7deg/s.

Fig. 10(e) shows the electromagnetic torque curves of the two rear-wheel drive motors of the vehicle. Due to the additional yaw moment, the electromagnetic torque outputs of the left and right motors have a torque difference. In combination with Fig. 11 (e) and (a), it could be seen that the difference between the left and right electromagnetic torques is equal to the additional yaw moment. In addition, it could be seen from Fig. 11 (e) and (b) that the variation trend of the electromagnetic torque is the same as that of the driving wheel torque. Since the reduction ratio of the wheel-side reducer in this research is set as 8, the driving torque is 8 times of the electromagnetic torque.

B. Simulations under DLC maneuver at middle speed

In order to verify the middle-speed handling stability of the distributed drive electric vehicle based on the electronic differential control strategy, simulations are also carried out in accordance with the standard operating conditions of DLC maneuvers of ISO3888-2:2002. Simulation conditions are set as follows: the vehicle speed is 90km/h, and the road adhesion coefficient is 0.85. The results are shown in Figure 11.

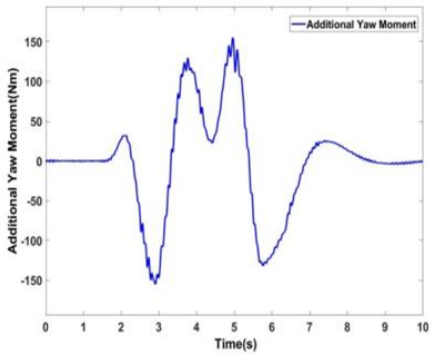

(a) Additional Yaw Moment

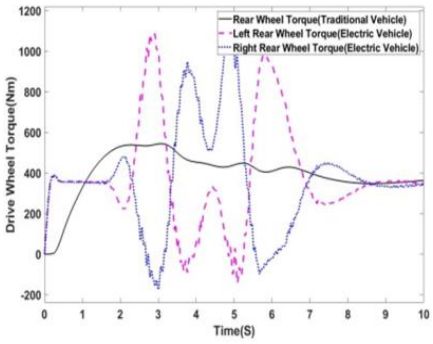

(b) Drive Wheel Torque

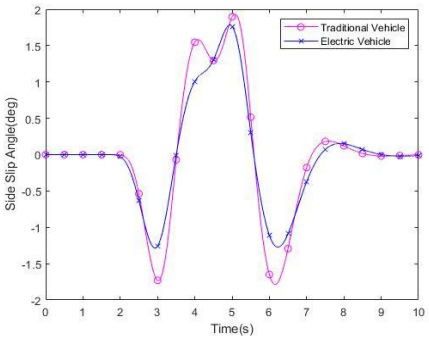

(c) Side Slip Angle

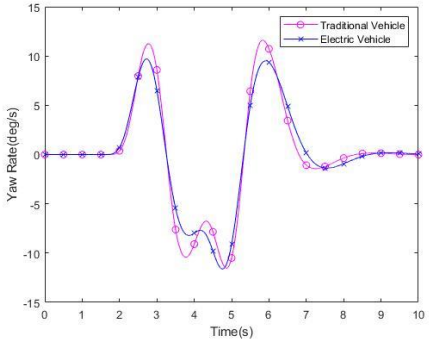

(d) Yaw Rate

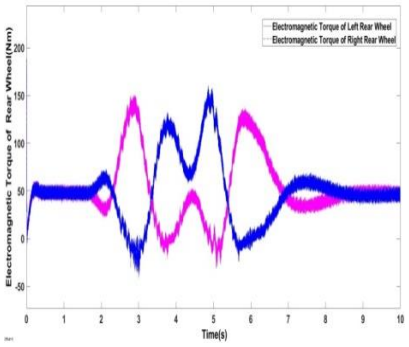

(e) Electromagnetic Torque of Rear Wheel

Fig.11: Simulation result comparisons of electronic differential control strategy under double lane change maneuver at middle speed.

TABLE Ⅶ: Comparisons of Simulation Results of Different Strategies under DLC Maneuver at 90km/h

Simulation Parameters	Mechanical differential	Electronic differential	
	Data	Data	Rate of change
β_{max}(deg)	1.93	1.91	-1.04%
ω_{rmax}(deg/s)	11.60	10.30	-11.20%

As can be seen from Fig. 11, under the 90km/h DLC maneuvers, both side slip angle and yaw rate of vehicle based on electronic differential are improved. From table VII, compared with the traditional mechanical differential, the change rate of vehicle yaw angular velocity based on electronic differential reaches -11.2%, which improves from the original 11.6deg/s to 10.3deg/s, and the side slip angle improves from the original 1.93deg to 1.91. The lateral stability of the vehicle is improved. Fig. 11(e) is the electromagnetic torque curves of the two rear-wheel drive motors of the vehicle. With the increase of the additional yaw moment, the output electromagnetic torque of the motor increases, and the difference between the left and right electromagnetic torque is equal to the value of the additional yaw moment.

C. Simulations under DLC maneuver at high speed

To verify the maneuverability and handling stability of distributed electric vehicles at high speeds based on the electronic differential control strategy, simulations are carried out in the standard operating conditions of DLC maneuvers. Test conditions are set as follows: the vehicle velocity is 120km/h, and the road adhesion coefficient is 0.85. The results are shown in Figure 12.

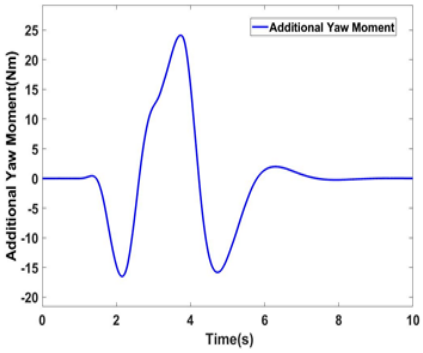

(a) Additional Yaw Moment

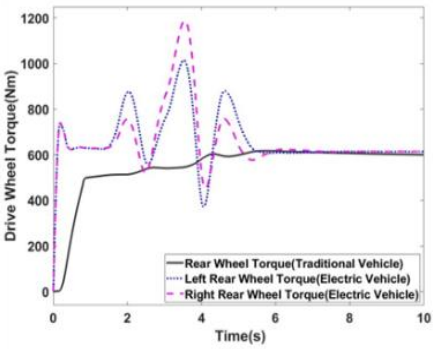

(b) Drive Wheel Torque

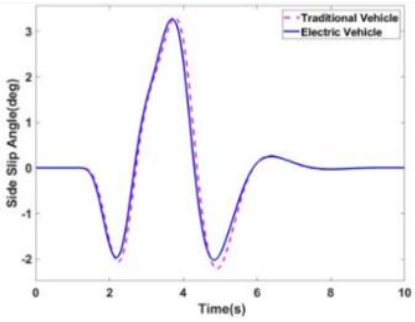

(c) Side Slip Angle

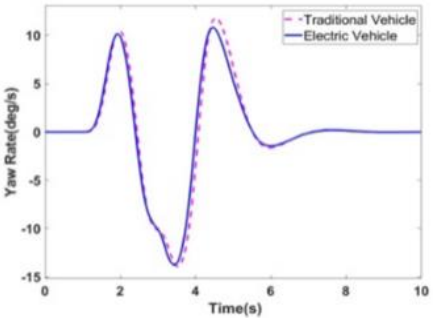

(d) Yaw Rate

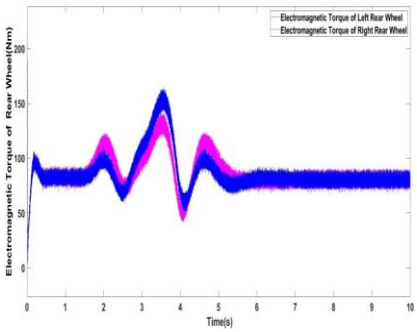

(e) Electromagnetic Torque of Rear Wheel

Fig.12: Simulation result comparisons of electronic differential control strategy under double lane change maneuver at high speed.

TABLE Ⅷ: Comparisons of Simulation Results of Different Strategies under DLC Maneuver at 120km/h

Simulation Parameters	Mechanical differential	Electronic differential	
	Data	Data	Rate of change
$\beta_{max}(deg)$	11.79	11.10	-5.9%
$\omega_{rmax}(deg/s)$	3.29	3.27	-0.61%

Fig.12 shows the vehicle motion states caused by two differential speed strategies under the 120km/h DLC, respectively. Fig.12(b) shows the trend of the driving torque under different strategies. The torque of the rear wheels based on the electronic differential strategy changes with the fluctuation of the additional yaw moment. As can be seen from Fig.12 (c) and (d), when the vehicle is running at high speed, the improvement of the lateral stability of the vehicle is not as obvious as that of the vehicle at medium and low speed, and the variation trend of the side slip angle and yaw rate of the vehicle brought by the electronic differential is almost the same as that of the traditional vehicle. This is because the rear wheel drive torque has reached the peak torque that PMSM could output after adjusting the additional yaw moment, and the motor has reached the maximum load. However, it can still achieve better differential effect.

D. Simulations in Step turn maneuver at middle speed

To verify the anti-skid performance of the electronic differential control strategy on the road with low adhesion coefficient, simulations are carried out with a step turn maneuver. The simulation conditions are set as follows: the vehicle velocity is 60km/h, the road adhesion coefficient is 0.13. The simulation analysis of the vehicle based on the electronic differential and the traditional mechanical differential are performed. The results are shown in Figure 13.

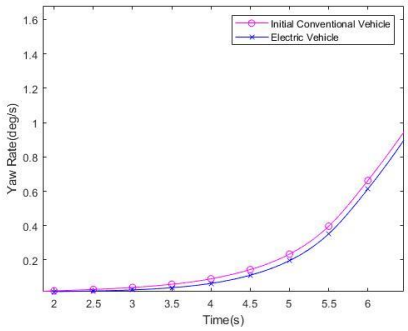

(a) Traditional Vehicle

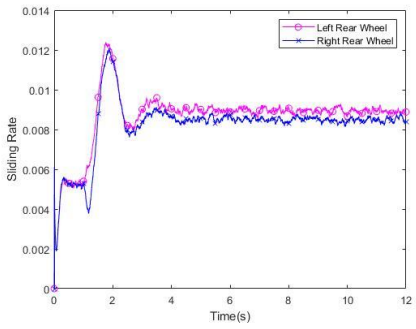

(b) Electric Vehicle

Fig.13: Simulation result comparisons of electronic differential control strategy under Step turn maneuver at middle speed

It can be seen from Figure 13 that when the vehicle based on a mechanical differential performs the step turn maneuver at a speed of 60km/h and the $\mu = 0.13$ on a road with a low adhesion coefficient, the wheels slip severely, and all four wheels reach a slip state within 8 seconds. However, the electronic differential-based vehicle has a sliding rate controller, which can redistribute the torque of the driving wheels on both sides when the wheels are about to slip, so that the sliding rate of each wheel is kept below 0.2, and at the same time, it can provide the vehicle with appropriate power, ensuring the driving safety of the vehicle.

V. CONCLUSIONS

Aiming at the electronic differential problem of distributed drive electric vehicles, this paper designs an electronic differential control strategy based on LQR torque distribution, and compares it with traditional mechanical differentials. The results show that:

(a) When the distributed drive electric vehicle is driving stably on a road with good adhesion coefficient, the LQR controller based on orthogonal experiment optimization can calculate the additional yaw moment according to the driver's intention, and adjust the torque

of the driving wheel in real time, which can achieve the differential effect while also improving the mobility and lateral stability of the vehicle.

(b) The sliding rate control strategy and torque distribution control strategy are designed based on the optimal sliding rate range. When the electric vehicle is running on a low adhesion coefficient road and is in an unstable state, the sliding rate controller can pass the feedback wheel sliding rate, quickly adjust the torque of the driving wheels until the vehicle returns to a stable state to restrain the vehicle from side slip.

REFERENCES

[1] YaDong Huang, Guifang Guo. A Review of Torque Distribution Strategies for Distributed Drive Electric Vehicles[J]. Automobile Applied Technology, 2020,45(22): 230-236+248.

[2] J. Folgado, S. S. Valtchev, F. Coito. Electronic differential for electric vehicle with evenly split torque[J]. IEEE International Power Electronics and Motion Control Conference, 2016:1204-1209.

[3] C. O. Luc á, F. R. Jos é and G. C. Alfonso. Electronic differential system for Light Electric Vehicles with two in-wheel motors[J]. International Conference on Renewable Energies and Power Quality, 2018:325-329.

[4] Ziqiang Tang, Xianwu Gong, Xuan Zhao, et al. Simulation research on self-adaptive differential of distributed drive electric vehicle[J]. Journal of Hefei University of Technology (Natural Science), 2017, 40(10):1320-1325.

[5] H. T. Al-Fiky, M. S. Asfoor, M. I. Yacoub, et al. Electronic Differential Optimization for Electric Vehicle Full Model for In-Wheel Permanent Magnet Brushless DC Motors[J]. IEEE International Conference on Control, Mechatronics and Automation, 2019:15-20.

[6] J. Folgado, S. S. Valtchev, F. Coito. Electronic differential for electric vehicle with evenly split torque[J]. 2016 IEEE International Power Electronics and Motion Control Conference,2016:1204-1209.

[7] F. J. L. Daya, P. Sanjeevikumar, F. Blaabjerg，et al. Analysis of Wavelet Controller for Robustness in Electronic Differential of Electric Vehicles: An Investigation and Numerical Developments[J]. Electric Power Components and Systems, 2016:1-11.

[8] R. C. B. Sampaio，A. C. Hernandes, M. Becker, et al. A New Control Architecture for Robust Controllers in Rear Electric Traction Passenger HEVs[J]. IEEE Transactions on Vehicular Technology, 2012:3441-3453.

[9] Yiding Hua, Haobin Jiang, Guoqing Geng. Electronic Differential Control of 2WD Electric VehicleConsidering Steering Stability[J]. AIP Conference Proceedings 1820, 2017:1-7.

[10] J. D. Setiawan, I. Haryanto, Munadi, et al. Modeling and Analysis of Lateral Control System on Electronic Differential for 2-Independent-Wheel Drive Electric Urban Bus[J]. 2018 5th International Conference on Electric Vehicular Technology, 2018.

[11] Yantao Tian, Xuanhao Cao, Xiaoyu Wang, et al. Four Wheel Independent Drive Electric Vehicle Lateral Stability Control Strategy[J]. IEEE/CAA Journal of Automatica Sinica, 2020:1403-1416.

[12] Dongbin Lu, Minggao Ouyang, Jing Gu, et al. Torque distribution algorithm for a permanent brushless DC hub motor for four-wheel drive electric vehicles[J]. Journal of Tsinghua University(Science and Technology), 2012,52(4):451-456.

[13] Zhuoping Yu, Jun Liu, Lu Xiong, et al. Control Strategies of Handling Improvement of Distributed Drive Electric Vehicle [J]. Journal of Tongji University (Natural Science), 2014,42(7):1088-1093.

[14] Ren He, Hang Yun. Electronic Diferential Control of Rear-Wheel Independent-Drive Electric Vehicle[J]. SAE International Journal of Vehicle Dynamics, Stability, and NVH, 2020:49-65.

[15] Zhisheng Yu. Theory of Automobile[M]. China Machine Press, 2009.

[16] Fan Yu, Yi Lin. Automotive System Dynamics[M]. China Machine Press, 2016.

[17] Yuping He, Md Manjurul Islam, Timothy D Webster. An Integrated Design Method for Articulated Heavy Vehicles with Active Trailer Steering Systems. SAE Int. J. Passeng. Cars – Mech. Syst. 3(1):158-174, 2010, https://doi.org/10.4271/2010-01-0092.

[18] Yuping He, Md. Manjurul Islam. An Automated Design Method for Active Trailer Steering Systems of Articulated Heavy Vehicles. J. Mech. Des. Apr 2012, 134(4):041002 (15 pages), https://doi.org/10.1115/1.4006047.

[19] Md. Manjurul Islam, Xuejun Ding, Yuping He. A Closed-loop Dynamic Simulation-based Design Method for Articulated Heavy Vehicles with Active Trailer Steering Systems. Vehicle System Dynamics, 2012, Vol. 50, No. 5, pp. 675-697.

[20] Jiali Tang, Zhangtao Xu. Analysis of Range and Analysis of Variance in Orthogonal Experiment [J]. Middle-school Mathematics, 2017(9): 31-34.

[21] Mutaz Keldani, Yuping He. Design of an Improved Robust Active Trailer Steering Controller for Multi-trailer Articulated Heavy Vehicles Using Software/Hardware-in-the-Loop Real-Time Simulations. In: Klomp M., Bruzelius F., Nielsen J., Hillemyr A. (eds) Advances in Dynamics of Vehicles on Roads and Tracks. IAVSD 2019. Lecture Notes in Mechanical Engineering. 2020, Springer, Cham. https://doi.org/10.1007/978-3-030-38077-9_162.

[22] Qiushi Wang, Yuping He. A Study on Single Lane-change Manoeuvres

for Determining Rearward Amplification of Multi-trailer Articulated Heavy Vehicles with Active Trailer Steering Systems. Vehicle System Dynamics, 2016, Vol. 54, No. 1, pp. 102-123.

Appendix 1. Notation and description of parameters of the thesis

Symbol	Description	Unit
u_d	Stator voltage of the direct axis	V
u_q	Stator voltage of the quadrature axis	V
R_s	Resistance of the stator	Ω
i_d	Stator current of the direct axis	A
i_q	Stator current of the quadrature axis	A
L_d	Inductive component of the direct axis	H
L_q	Inductive component of the quadrature axis	H
ω_e	Electrical angular velocity	rad/s
ω_m	Angular velocity of rotation	rad/s
ψ_f	Permanent Magnet Flux Linkage	Wb
ψ_d	Stator flux linkage of the direct axis	Wb
ψ_q	Stator flux linkage of the quadrature axis	Wb
T_e	Electromagnetic Torque	Nm
T_L	Load Torque	Nm
P_n	The number of pole-pairs	
J	Moment of Inertia	$kg \cdot m^2$
B	Damping Factor	$N \cdot m \cdot s$
k_1	Cornering stiffness of the front axle	N/rad
k_2	Cornering stiffness of the rear axle	N/rad
a	Longitudinal distance from the CG of the vehicle whole mass to the front axle	m
b	Longitudinal distance from the CG of the vehicle whole mass to the rear axle	m
ω_r	Yaw rate at the CG of the vehicle	rad/s
β	Side-slip angle at the CG of the vehicle	rad
m	Total mass of the vehicle	kg
I_z	Moment of inertia of the vehicle about yaw axis	$kg \cdot m^2$
δ	Steer angle of the front wheels	rad
u	Longitudinal speed at the CG of the vehicle	m/s
v	Lateral speed at the CG of the vehicle	m/s
β_d	Desired side-slip angle at the CG of the vehicle	rad
ω_{rd}	Desired yaw rate at the CG of the vehicle	rad/s
$\Delta\beta$	The error between β and β_d	rad
$\Delta\omega_r$	The error between ω_r and ω_{rd}	rad/s
V_x	Longitudinal speedSpeed at the CG of the vehicle	m/s
V_x'	Desired speed at the CG of the vehicle	m/s
ΔM_z	Additional yaw moment	Nm
ω_{fl}	Rotating speed of the front left wheel	rpm
ω_{fr}	Rotating speed of the front right wheel	rpm
ω_{rl}	Rotating speed of the rear left wheel	rpm
ω_{rr}	Rotating speed of the rear right wheel	rpm

Symbol	Description	Unit
s_{rl}	Slip rate of the rear left wheel	
s_{rr}	Slip rate of the rear right wheel	
α_{rl}	Torque correction coefficient of the rear left wheel	
α_{rr}	Torque correction coefficient of the rear right wheel	
T_{rl1}	The target torque of the first assignment of the rear left wheel	Nm
T_{rr1}	The target torque of the first assignment of the rear right wheel	Nm
T_{rl2}	The target torque of the second assignment of the rear left wheel	Nm
T_{rr2}	The target torque of the second assignment of the rear right wheel	Nm
T_{rl}	The target torque of the rear left wheel	Nm
T_{rr}	The target torque of the rear right wheel	Nm